BRD9 regulates interferon-stimulated genes during macrophage activation via cooperation with BET protein BRD4

Nasiha S. Ahmed[a,1], Jovylyn Gatchalian[a,1], Josephine Ho[a], Mannix J. Burns[a], Nasun Hah[b], Zong Wei[c], Michael Downes[d], Ronald M. Evans[d], and Diana C. Hargreaves[a,2]

[a]Molecular and Cell Biology Laboratory, Salk Institute for Biological Studies, La Jolla, CA 92037; [b]Chapman Foundations Genomic Sequencing Core, Salk Institute for Biological Studies, La Jolla, CA 92037; [c]Department of Physiology and Biomedical Engineering, Mayo Clinic Arizona, Scottsdale, AZ 85249; and [d]Gene Expression Laboratory, Salk Institute for Biological Studies, La Jolla, CA 92037

Edited by Vishva Dixit, Physiological Chemistry, Genentech, San Francisco, CA; received June 10, 2021; accepted November 9, 2021

Macrophages induce a number of inflammatory response genes in response to stimulation with microbial ligands. In response to endotoxin Lipid A, a gene-activation cascade of primary followed by secondary-response genes is induced. Epigenetic state is an important regulator of the kinetics, specificity, and mechanism of gene activation of these two classes. In particular, SWI/SNF chromatin-remodeling complexes are required for the induction of secondary-response genes, but not primary-response genes, which generally exhibit open chromatin. Here, we show that a recently discovered variant of the SWI/SNF complex, the noncanonical BAF complex (ncBAF), regulates secondary-response genes in the interferon (IFN) response pathway. Inhibition of bromodomain-containing protein 9 (BRD9), a subunit of the ncBAF complex, with BRD9 bromodomain inhibitors (BRD9i) or a degrader (dBRD9) led to reduction in a number of interferon-stimulated genes (ISGs) following stimulation with endotoxin lipid A. BRD9-dependent genes overlapped highly with a subset of genes differentially regulated by BET protein inhibition with JQ1 following endotoxin stimulation. We find that the BET protein BRD4 is cobound with BRD9 in unstimulated macrophages and corecruited upon stimulation to ISG promoters along with STAT1, STAT2, and IRF9, components of the ISGF3 complex activated downstream of IFN-alpha receptor stimulation. In the presence of BRD9i or dBRD9, STAT1-, STAT2-, and IRF9-binding is reduced, in some cases with reduced binding of BRD4. These results demonstrate a specific role for BRD9 and the ncBAF complex in ISG activation and identify an activity for BRD9 inhibitors and degraders in dampening endotoxin- and IFN-dependent gene expression.

inflammation | macrophages | BRD9 | bromodomain protein 9 | BRD4

Mac rophages are a critical cell type of the innate immune system that respond to microbial ligands and cytokines by inducing a transcriptional program of proinflammatory and effector genes. These genes include signaling and transcription factors, cell-surface receptors, cytokines, anti-microbial effectors, and other genes that facilitate the activation of the adaptive immune system and pathogen clearance. The kinetics of activation and resolution of these genes are therefore precisely regulated in order to coordinate the appropriate immune response. Epigenetic regulation is an important mechanism by which these transcriptional events are controlled.

Toll-like receptor 4 (TLR4) activation in response to lipopolysaccharide (LPS) or Lipid A leads to the engagement of adapter proteins MyD88 and TRIF, which activate transcription factors in the NF-κB, AP-1, and IRF families (1). These factors initiate a transcriptional cascade, which begins with the very rapid transcription of primary-response genes (PRGs). PRGs facilitate the activation of secondary-response genes (SRGs), which are defined by their requirement for protein synthesis and the failure to be induced in the presence of cycloheximide (CHX) (2, 3). Indeed, the induction of the PRG *Ifnb1* downstream of TRIF/IRF3 activation results in secretion of interferon-beta (IFN-β) and autocrine-signaling through IFN-alpha (IFN-α) Receptor (IFNAR), driving much of the secondary response (2, 4). Consistent with their very rapid activation, PRGs are generally accessible, marked by active histone modifications, loaded with paused RNA Polymerase II, and regulated by transcriptional elongation (3, 5, 6). In contrast, SRGs and a subset of PRGs, so-called late PRGs, require chromatin-remodeling by the SWI/SNF chromatin-remodeling complex as knockdown of the SWI/SNF ATPase subunits BRG1 and BRM results in failure to induce SRGs and late PRGs, with no effect on PRGs (7, 8).

SWI/SNF complexes are large, multisubunit complexes that utilize ATP to provide chromatin accessibility for transcription factors and other epigenetic regulators. At least three major variants of the complex exist, called canonical BAF (cBAF), polybromo BAF (PBAF), and the recently discovered noncanonical BAF (ncBAF) complex, also known as the GBAF complex, which uniquely incorporates the bromodomain-containing protein BRD9 and GLTSCR1 or GLTSCR1L (9–11). We and others have shown that the BAF, PBAF, and ncBAF variants

Significance

Macrophages regulate many aspects of the innate immune response and the activation of adaptive immunity following exposure to microbial ligands. However, macrophages can also contribute to inflammation underlying diseases such as atherosclerosis and obesity. Epigenetic regulators control inflammatory gene regulation and, as such, are potential targets for modulation of the inflammatory response. Here, we show that inhibitors and degraders of the bromodomain protein BRD9, a subunit of the noncanonical BAF complex, limit inflammation by specifically blocking the induction of interferon-stimulated genes. This effect overlaps with the transcriptional responses with the BET inhibitor JQ1 but affects fewer genes and is more specific in scope. Our results suggest that BRD9 inhibitors/degraders may be therapeutically relevant agents to limit interferon-associated inflammation.

Author contributions: N.S.A., J.G., J.H., and D.C.H. designed research; N.S.A., J.G., J.H., M.J.B., and D.C.H. performed research; N.H., Z.W., M.D., and R.M.E. contributed new reagents/analytic tools; N.S.A., J.G., J.H., and D.C.H. analyzed data; and N.S.A., J.G., and D.C.H. wrote the paper.

The authors declare no competing interest.

This article is a PNAS Direct Submission.

[1]N.S.A. and J.G. contributed equally to this work.

[2]To whom correspondence may be addressed. Email: dhargreaves@salk.edu.

This article contains supporting information online at http://www.pnas.org/lookup/suppl/doi:10.1073/pnas.2110812119/-/DCSupplemental.

Published December 30, 2021.

differ in their localization to genetic regulatory elements, with BAF complexes being primarily enriched at enhancers, while ncBAF complexes are found in greater proportion at promoters and CTCF/cohesion-bound sites (10–12). Our work has defined specific relationships between ncBAF complexes and transcription factors in embryonic stem (ES) cells, β cells, and T regulatory cells (Tregs) that underlie a requirement for BRD9 in naıve pluripotency (10), β cell inflammation (13), and Treg suppression (14), respectively.

Here, we made use of two BRD9 bromodomain inhibitors [I-BRD9 (15) and BI-9564 (16)] and a BRD9 degrader (dBRD9) (17) to examine the role of BRD9 and ncBAF complexes in inflammatory gene expression induced downstream of TLR4 upon stimulation with Lipid A in bone marrow–derived macrophages (BMDMs). Our analysis identified a requirement for BRD9 for induction of inflammatory genes in the IFN-α/β and IFN-γ pathways, also known as IFN-stimulated genes (ISGs), despite normal activation of PRGs. BRD9-dependent genes were highly correlated with genes disrupted by treatment with BET protein inhibitor, JQ1 (18), which inhibits BRD2, BRD3, and BRD4. Mechanistically, we find that BRD9 and BRD4 are cobound in unstimulated macrophages and corecruited to new sites upon Lipid A stimulation. BRD9/BRD4 cogained sites are enriched for IRF motifs, and we observe strong overlap at promoters with binding of STAT1, STAT2, and IRF9, which together constitute the ISGF3 complex that is activated in response to IFN-α/β stimulation (19, 20). Treatment with BRDi or dBRD9 results in reduction in ISGF3 binding at BRD9/BRD4 cobound sites. Our results suggest that ncBAF complexes work with BRD4 to regulate a specific arm of the TLR4-induced response, namely genes induced following autocrine-signaling via IFNAR, through stabilization of the ISGF3 transcriptional complex.

Results

BRD9 Inhibition and Degradation Affects Induction of a Subset of BET Protein-Dependent Inflammatory Genes Following Lipid A Stimulation. To address whether BRD9 regulates gene expression following endotoxin stimulation in macrophages, we performed RNA sequencing (RNA-seq) on BMDMs pretreated with vehicle (dimethyl sulfoxide, DMSO), I-BRD9, or BI-9564 (collectively, BRD9i) or dBRD9 for 18 to 24 h and then stimulated with Lipid A for 0, 1, or 4 h. We chose these inhibitors based on their reported specificity for BRD9 and selectivity for the BRD9 bromodomain over the highly related bromodomain of BRD7 (a subunit of the PBAF complex) and bromodomain 1 of the BET proteins (15, 16). dBRD9 is a heterobifunctional molecule that bridges a related BRD9 bromodomain inhibitor, BI-7273, with the cereblon E3 ubiquitin ligase complex and is also specific for BRD9 (17). Additionally, we wished to compare the effects of different BRD9 bromodomain inhibitors and BRD9 protein degradation. Based on our work and others demonstrating a biochemical interaction between BRD9 and the BET proteins BRD4 (9, 10, 12, 21) and BRD2 (12) and a similar effect of BRD9 and BET protein inhibition on transcription in other systems (10, 12), we included an additional treatment with JQ1 (18), a BET bromodomain inhibitor, in our studies.

Based on previous literature implicating a role for BRG1/BRM in induction of SRGs (7, 8), we first performed an analysis based on the kinetics of gene activation. We identified 1,242 genes up-regulated by at least fourfold in Lipid A-stimulated BMDMs and differentially expressed in inhibitor-treated cells by 1.5-fold compared to vehicle at any timepoint, which we then subjected to k-means clustering (Fig. 1*A*). Clusters 7 and 9 contain PRGs that have maximal induction at 1 h in vehicle. Clusters 1, 2, 5, 6, and 10 contain genes that are maximally activated at 4 h in vehicle, which are likely SRGs. We found that treatment with BRD9i, JQ1, and dBRD9 resulted in dampened induction of genes in clusters 1, 2, and 5, suggesting that BRD9 and BET proteins regulate SRGs (Fig. 1*A*). Notably, while the inhibitors had a similar effect on the induction of inflammatory genes in these clusters, the effects of I-BRD9 and JQ1 were more pronounced compared to dBRD9 and BI-9564. There were substantially more differentially expressed genes (DEGs, fold-change [FC] 1.5, Benjamini–Hochberg adjusted P value < 0.05) for both I-BRD9 (n = 4,464) and JQ1 (n = 4,026) compared to dBRD9 (n = 805) and BI-9564 (n = 470). In total, 256 and 327 DEGs were commonly regulated by all four inhibitors at 1 h and 4 h post Lipid A stimulation, respectively (Fig. 1*B*). We then plotted the log2 fold change of RNA expression with BRD9i/dBRD9 compared to JQ1 and observed a positive correlation for each treatment against JQ1, suggesting that BRD9 and BET proteins cooperate in transcriptional regulation of inflammatory genes (Fig. 1 *C* and *D*). Notably, most DEGs are down-regulated by inhibitor treatment, in agreement with the cluster results showing dampened induction of genes 4 h post Lipid A stimulation. Finally, to determine how well each BRD9 inhibitor treatment correlated with Brd9 genetic deletion, we made use of an RNA-seq dataset comparing LPS + IFN-γ treatment in BMDM derived from wild-type or *Brd9f/f;LysM-Cre* animals, in which Brd9 is conditionally deleted in the myeloid lineage (22). Using gene set enrichment analysis (GSEA), we found that genes down-regulated in BI-9564-, dBRD9-, and I-BRD9-treated Lipid A-induced macrophages were positively correlated with genes down-regulated in LPS+IFN-γ–treated Brd9 knockout macrophages with normalized enrichment scores (NES) of 2.47, 2.33, and 2.35, respectively (Fig. 1*E*).

BRD9 Inhibition/Degradation Reduces IFNAR-Dependent Gene Expression. To determine what pathway is particularly affected by inhibiting BRD9, we compared our RNA-seq data with publicly available datasets that include genetic deletions of key players in the TLR4 pathway: MYD88, TRIF, IRF3, and IFNAR (2). Additionally, we used datasets in which BMDMs were treated with CHX prior to LPS stimulation as well as PAM3CSK4, which is a TLR2 agonist that activates NF-κB but not IRF3 (2).

Using the same gene clusters from Fig. 1*A*, we plotted the percent gene induction compared to wild-type or untreated in each of the datasets (Fig. 2*A*). All of the genes included in our analysis were affected by MYD88 and TRIF deletions. Clusters 1, 2, and 5, which contained our genes of interest, represent a subset of CHX-affected genes, confirming that BRD9i/dBRD9- and JQ1-dependent genes are SRGs. Clusters 1, 2, and 5 were also affected by IRF3 and IFNAR deletions and failed to be induced by PAM3CSK4, strongly suggesting that BRD9 and BET proteins coregulate the IRF3- and IFNAR-dependent response in macrophages. In agreement with this, GSEA of BRD9-dependent DEGs in 4-h Lipid A stimulation identified IFN-γ and IFN-α responses as the most-significant GSEA Hallmark pathways (Fig. 2*B*). We examined the log2 fold change of ISGs annotated to the IFN-γ and IFN-α pathways and found a reduction in essentially all of these genes following I-BRD9 or JQ1 treatment. The effect of BI-9564 and dBRD9 was less pronounced, but also revealed a consistent down-regulation across both inhibitors for a number of IFNAR-dependent genes (Fig. 2*C*). To determine how specific the effect of BRD9i or dBRD9 is for the induction of ISGs, we made use of a public data set defining IFNAR-independent PRGs and SRGs (2). We saw variable effect of the inhibitors on these genes: PRGs such as *Tnf*, *Ccl2*, and *Cxcl1* were expressed at normal levels or hyperactivated in all inhibitor conditions. In contrast, a number of IFNAR-independent SRGs were affected by I-BRD9 and JQ1, including *Il6* and *Il12b*, while BI-9564 and dBRD9 by and large had no effect on the expression of IFNAR-independent

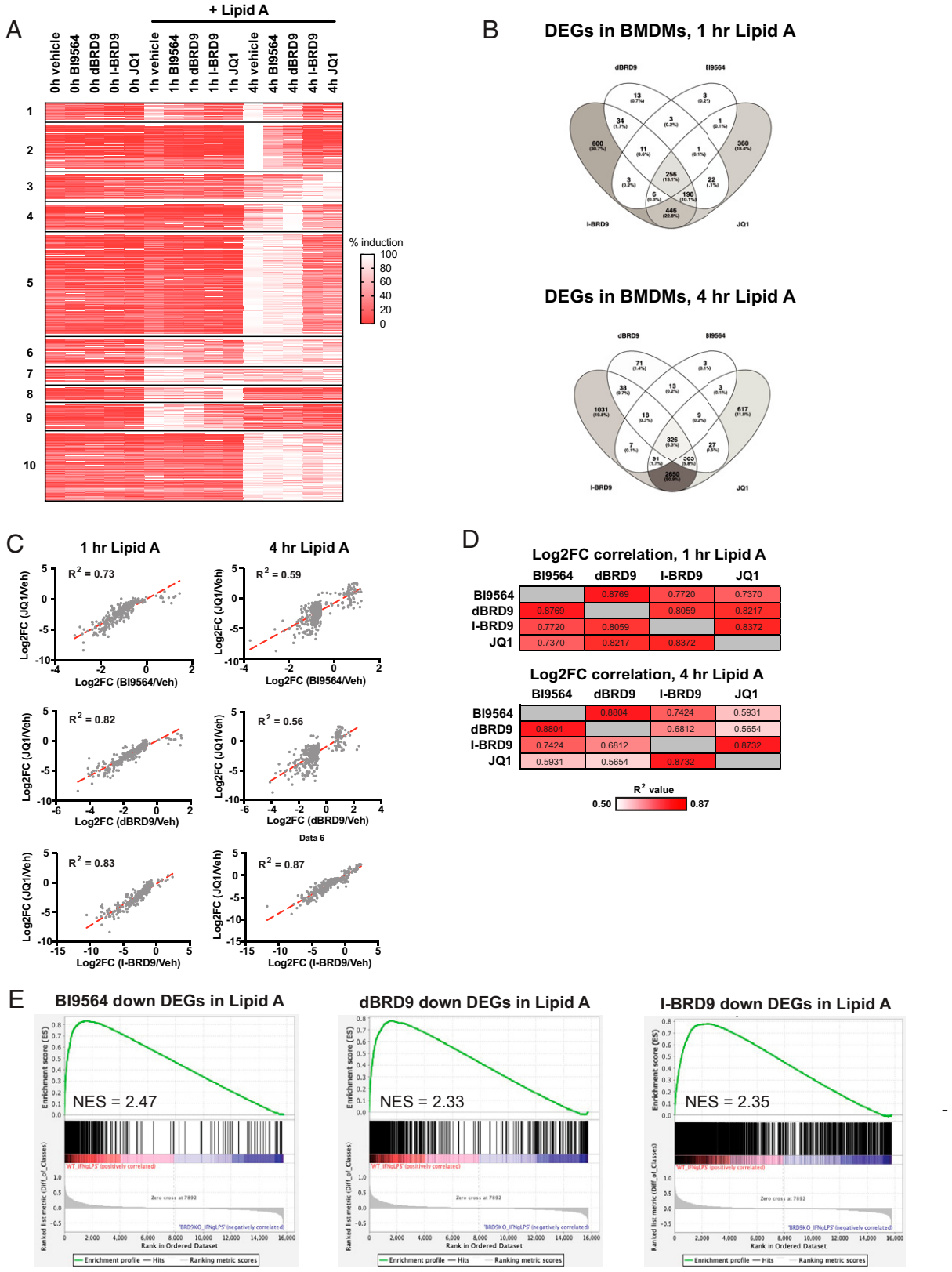

Fig. 1. BRD9 inhibition or degradation reduces induction of Lipid A-stimulated genes. (*A*) K-means clustering of genes that get up-regulated by fourfold after 1 h or 4 h of Lipid A stimulation over vehicle and that get differentially expressed by 1.5-fold with BI9564, dBRD9, I-BRD9, or JQ1 treatment over vehicle. (*B*) Butterfly Venn diagram of DEGs in BI9564-, dBRD9-, I-BRD9-, or JQ1-treated groups compared to vehicle in 1 h and 4 h Lipid A-stimulated conditions. (*C*) Scatterplots of RNA-seq log2 fold change (Log2FC) over vehicle in BI-9564-, dBRD9-, or I-BRD9-treated groups compared to JQ1 in either 1 h (*Left*) or 4 h (*Right*) Lipid A-stimulated conditions. R^2 indicates goodness of fit after linear regression analysis. (*D*) Matrix showing R^2 values for each RNA-seq log2FC dataset comparison. (*E*) GSEA enrichment plots of significantly down-regulated BI-9564, dBRD9, or I-BRD9 DEGs in 4 h Lipid A compared to wild-type or *Brd9f/f:LysMCre* BMDMs treated with LPS and IFN-γ. Normalized enrichment scores (NES) for each plot are shown.

genes (Fig. 2*D*). Only *Il10*, *Saa3*, and *Snn* were reduced among IFNAR-independent genes in the BI-9564 and dBRD9 conditions (Fig. 2*D*). These results indicate that while I-BRD9 and JQ1 affect SRGs generally, BI-9564 and dBRD9 selectively affect IFNAR-dependent SRGs.

Reduced expression of ISGs with BRD9i/dBRD9 could be due to reduced autocrine-signaling through IFNAR owing to reduced induction of *Ifnb1* or reduced expression of IFNAR pathway components or, alternatively, direct effects on ISG induction downstream of IFNAR-signaling. We found no effect of BI-9564 or dBRD9 on the expression of the *Ifnb1* gene or IFN-β reporter activity as measured by the RAW-Dual (IRF-Lucia/KI-[MIP-2]SEAP) reporter line, in which luciferase is under the control of an ISRE promoter element (Fig. 2 *C* and *E*). In contrast, I-BRD9 and JQ1 significantly affected *Ifnb1* induction and IFN-β reporter activity (Fig. 2 *C* and *E*). Further, components of the IFNAR pathway, including *Ifnar1*, *Ifnar2*, *Stat1*, *Stat2*, and *Irf9*, were down-regulated in I-BRD9 and JQ1 but not BI-9564 or dBRD9 conditions. Western blot analysis indicated that induction of IRF9 and STAT2 proteins upon Lipid A stimulation was compromised in I-BRD9- and JQ1-treated cells but induced normally in dBRD9-treated cells (Fig. 2*F*). These data indicate that ISG expression in I-BRD9- and JQ1-treated cells is likely affected by the reduced expression of *Ifnb1* and IFNAR pathway components necessary for Type I IFN-signaling. In contrast, reduced ISG induction in the context of BI-9564 and dBRD9 is likely due to factors downstream of IFNAR-signaling. To test this directly, we performed RNA-seq on BMDM following IFN-α stimulation with or without dBRD9 treatment and found that genes that are down-regulated in BI-9564- or dBRD9-treated Lipid A-stimulated BMDMs are positively correlated with genes that are down-regulated by dBRD9 treatment in IFN-α stimulated BMDMs (Fig. 2*G*). These data suggest that BRD9 is required for IFNAR-induced ISG transcription following direct stimulation with type I IFN, and this function of BRD9 is the basis for the reduced induction of ISGs in dBRD9- or BI-9564-treated, Lipid A-stimulated conditions in which autocrine type I IFN-signaling occurs.

BRD9i/dBRD9 Affect BRD9 and BRD4 Corecruitment to Chromatin in Response to Lipid A. To determine whether BRD9 cooperates with BET proteins to regulate transcription in Lipid A-stimulated macrophages, we performed chromatin immunoprecipitation followed by sequencing (ChIP-seq) for BRD9 and the BET proteins BRD4 and BRD2 in the macrophage cell line RAW264.7 in unstimulated and 4-h Lipid A-stimulated conditions. We focused on BRD4 and BRD2, because these proteins and not BRD3 were shown to interact biochemically with BRD9 (9, 10, 12). Additionally, *Brd4* and *Brd2* genetic deletion decreases macrophage inflammatory response to LPS stimulation (23, 24). However, despite overlap of BRD9, BRD4, and BRD2 ChIP-seq peaks in unstimulated and Lipid A-stimulated RAW264.7, at BRD9 Lipid A-gained sites, we observed increased binding of BRD4 but not BRD2 (*SI Appendix*, Fig. S1 *A* and *B*), suggesting that BRD9 primarily collaborates with BRD4 in the context of Lipid A stimulation. BRD9 sites were strongly enriched for the CTCF motif in unstimulated cells, similar to what we and others have observed in other cell systems (10–12), which was more significant at BRD9 sites than BRD9/BRD4 cobound sites (*SI Appendix*, Fig. S1*C*). Following stimulation, we observed increased significance of motifs of various stimulus-regulated transcription factors, including AP-1 and IRF motifs, for BRD9 alone and BRD9/BRD4 cobound sites. These epigenomic data point to the specific corecruitment of BRD9 and BRD4 to new sites in response to stimulus-responsive transcription factors following Lipid A stimulation.

We then sought to understand how BRD9i/dBRD9 affect the binding of BRD9 and BRD4 in BMDMs. Similar to RAW264.7s, we observed cobinding of BRD9 and BRD4 in unstimulated BMDMs and corecruitment of BRD9 and BRD4 to new sites in response to Lipid A stimulation. BI-9564 and I-BRD9 caused displacement of BRD9 at several thousand sites, while dBRD9 caused widespread loss of BRD9-binding (Fig. 3*A*). Over 3,000 lost BRD9 sites were shared in all three BRD9 inhibitor treatment conditions (Fig. 3*B*). Further, JQ1 resulted in BRD9 displacement at 9,462 sites, confirming our previous findings in ES cells that BET inhibition results in loss of BRD9 binding (10). Conversely, BI-9564 and dBRD9 resulted in BRD4 displacement at 1,632 and 1,919 sites, respectively, while I-BRD9 mirrored the effects of JQ1 on BRD4-binding, resulting in loss of over 8,500 BRD4 sites (Fig. 3*C*). Thus, BI-9564 and dBRD9 preferentially affect BRD9-binding but also result in loss of BRD4-binding at a subset of sites (Fig. 3 *D* and *E*). I-BRD9, in contrast, results in widespread displacement of both BRD9 and BRD4, behaving similarly to JQ1 (Fig. 3 *D* and *E*).

Finally, we assessed the correlation between BRD9/BRD4 displacement and gene expression in the context of each treatment. We found that BRD9 was preferentially lost at BI-9564- and dBRD9-affected DEGs, with a subset of DEGs exhibiting reduced binding of both BRD9 and BRD4 at cobound sites (colost, stripes), indicating that BRD9 loss is correlated with the changes in gene expression in BI-9564/dBRD9-treated cells (Fig. 3*F*). In contrast, BRD9- and BRD4-binding were both individually affected at I-BRD9- and JQ1-affected DEGs (lost, polka dots) in addition to being colost at a number of DEGs (colost, stripes) (Fig. 3*F*). These data suggest that the transcriptional effects of I-BRD9 and JQ1 could be due to reduced binding of BRD9 and/or BRD4. Interestingly, DEGs that lost either BRD9 alone or BRD9/BRD4 in one or more treatment were enriched in the IFN-γ and IFN-α response pathways (Fig. 3*G*). Thus, the effects of BRD9i/dBRD9/JQ1 on BRD9-binding and its cobinding with BRD4 underscore the correlation between BRD9 or BET protein inhibition in Lipid A-induced transcription.

BRD9/BRD4 Cogained Sites Are Enriched for Binding of the ISGF3 Transcription Factor Complex. Motif analysis of BRD9/BRD4 cogained sites revealed an enrichment of IRF3(IRF), JunB (bZIP), and p65 motifs as well as macrophage lineage-determining transcription factors, PU.1 and CEBP (Fig. 4*A*). The strong enrichment for IRF motif suggested that BRD9 and BRD4 may regulate IRF family members IRF3 and/or IRF9 and its associated factors STAT1 and STAT2. We performed ChIP-seq of IRF9, STAT1, and STAT2 in unstimulated and 4-h Lipid A conditions in BMDMs. We then overlaid BRD9, BRD4, and BRD9/BRD4 cogained sites with our in-house generated ISGF3 ChIP-seq data, in addition to publicly available ChIP-seq data of IRF3 (Lipid A) (2), PU.1 (LPS) (25), p65 (LPS) (26), and ISGF3 (IFN-β) (19). Cobinding enrichment analysis indicated that BRD9/BRD4 cogained sites were enriched with IRF transcription factors IRF3 and IRF9, with comparatively less enrichment for PU.1 (Fig. 4*B*). However, given that IRF3-dependent transcription of *Ifnb1* was normal following BI-9564 and dBRD9 treatment, we followed up on the cobinding of BRD9/BRD4 with ISGF3. At BRD9 Lipid A-gained sites, we observed BRD4-binding in both unstimulated and stimulated conditions, with increased binding at BRD9 Lipid A-gained sites after stimulation. ISGF3-binding was also regulated by stimulation and was increased at BRD9 gained sites following Lipid A or IFN-β stimulation (Fig. 4*C*).

Genomic annotation of BRD9 and BRD4 Lipid A-gained sites showed an enrichment of intergenic and intronic regions along with a small fraction of sites annotated to promoters (Fig. 4*D*). In contrast, ISGF3, BRD9, and BRD4 cobound sites exhibited a notable proportion of promoter-bound sites, with 26% and 23% of sites annotating to promoters following Lipid

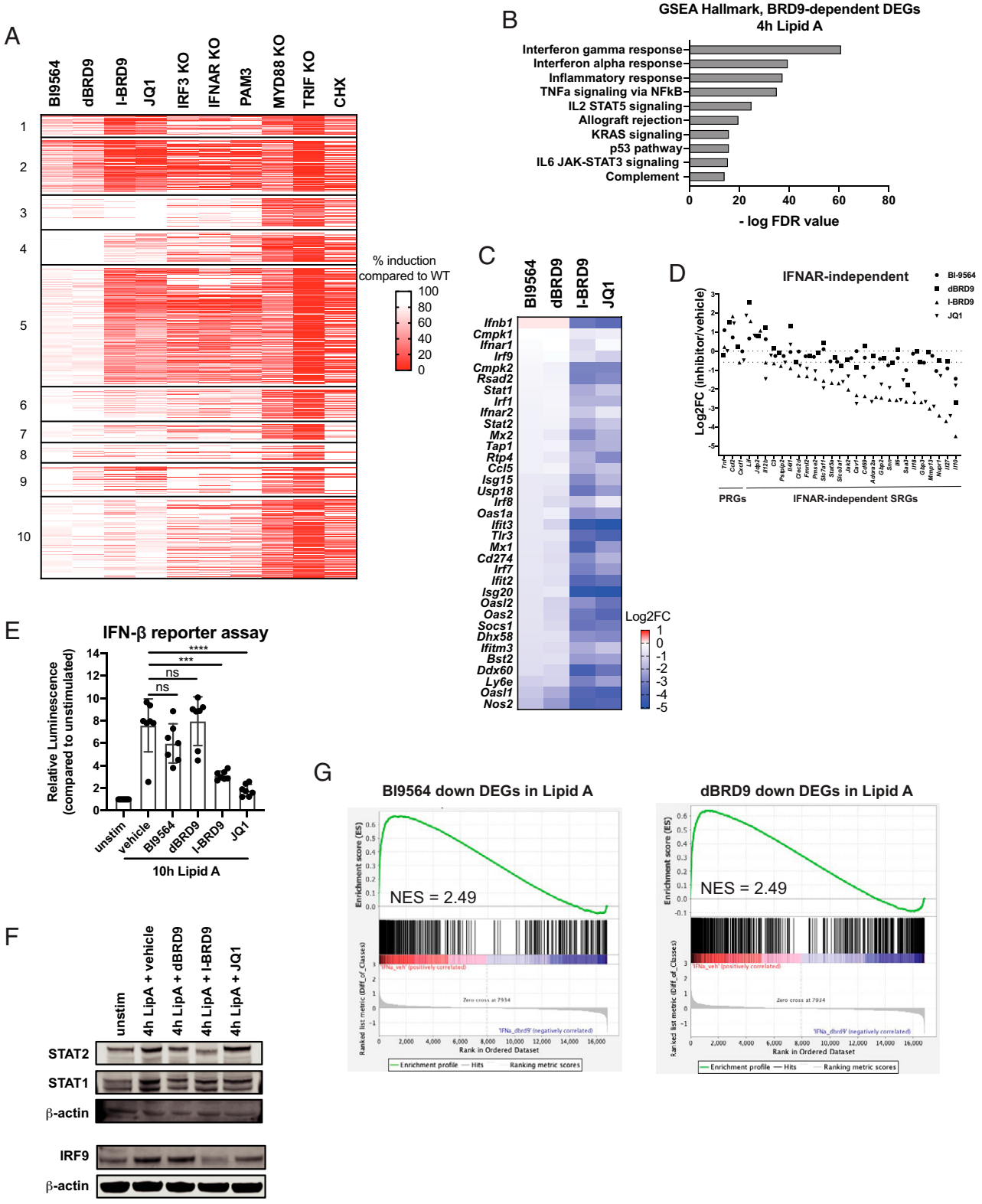

Fig. 2. BRD9 inhibition or degradation reduces the induction of ISGs in Lipid A or IFN-α stimulated BMDMs. (*A*) Heat map showing the percent induction compared to wild-type or untreated in LPS or Lipid A stimulation in the different datasets. The different gene clusters are presented as in Fig. 1*A*. (*B*) Bar graph showing enrichment of BRD9-dependent genes in 4-h Lipid A condition against the indicated GSEA Hallmark gene sets. (*C*) RNA-seq Log2FC values for genes in the IFN-γ and IFN-α response pathways in BI9564-, dBRD9-, I-BRD9-, or JQ1-treated groups compared to vehicle after 4 h of Lipid A stimulation. (*D*) Log2FC of BI9564, dBRD9, I-BRD9, or JQ1 over vehicle condition of PRGs and IFNAR-independent genes in 4 h Lipid A-stimulated BMDMs. (*E*) GSEA enrichment plots of significantly down-regulated BI-9564 and dBRD9 DEGs in 4 h Lipid A compared to dBRD9 DEGs in IFN-α-treated BMDMs. Normalized enrichment scores (NES) for each plot are shown. (*F*) Luciferase assay of IFN-β activity in RAW-Dual macrophages in supernatants from BMDMs treated with inhibitors and stimulated for 10 h with Lipid A. (*G*) Representative Western blot for STAT1, STAT2, and IRF9 in unstimulated versus Lipid A-stimulated BMDMs with vehicle, dBRD9, I-BRD9, or JQ1. β-actin is used as loading control.

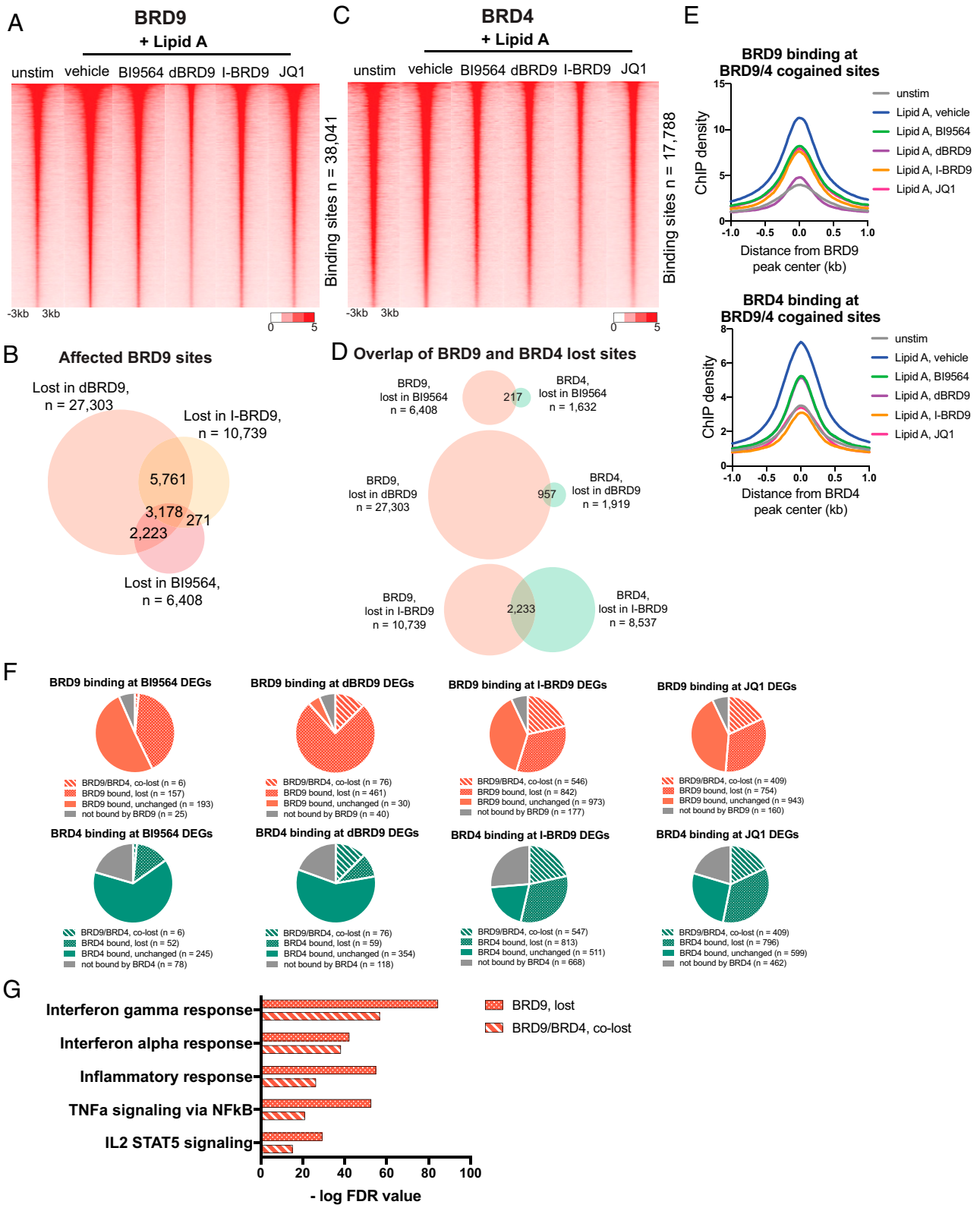

Fig. 3. BI-9564, dBRD9, and I-BRD9 have different effects on BRD9 and BRD4 chromatin binding. (*A*) Heat map of BRD9 ChIP signal in the presence of BRDi ± 3 kilobases (kb) centered on the BRD9 peak, ranked according to BRD9 read density at BRD9-bound sites in Lipid A-stimulated BMDMs. (*B*) Venn diagrams showing the overlap of differentially lost BRD9 ChIP-seq sites in BRD9i treatment in Lipid A-stimulated conditions. (*C*) Heat map of BRD4 ChIP signal in the presence of BRDi ± 3 kilobases (kb) centered on the BRD4 peak, ranked according to BRD4 read density at BRD4 bound sites in Lipid A-stimulated BMDMs. (*D*) Venn diagram of the overlap of BRD9 and BRD4 lost sites in BI-9564, dBRD9, and I-BRD9 treatment in Lipid A-stimulated BMDMs. (*E*) Histograms of BRD9 and BRD4 ChIP-seq tag density in the presence of BRDi treatment ± 1 kb, centered on sites that cogain binding for BRD9 and BRD4 in Lipid A-stimulated conditions. (*F*) Pie chart showing the number of BI-9564, dBRD9, I-BRD9, or JQ1 DEGs that are BRD9 bound (orange) or BRD4 bound (green) in Lipid A and that significantly lose BRD9, BRD4, or both BRD9 and BRD4 at a cobound site upon BRDi treatment (*G*) Bar graph showing enrichment of DEGs that lost either BRD9 alone or BRD9/BRD4 in one or more treatment against indicated GSEA Hallmark gene sets..

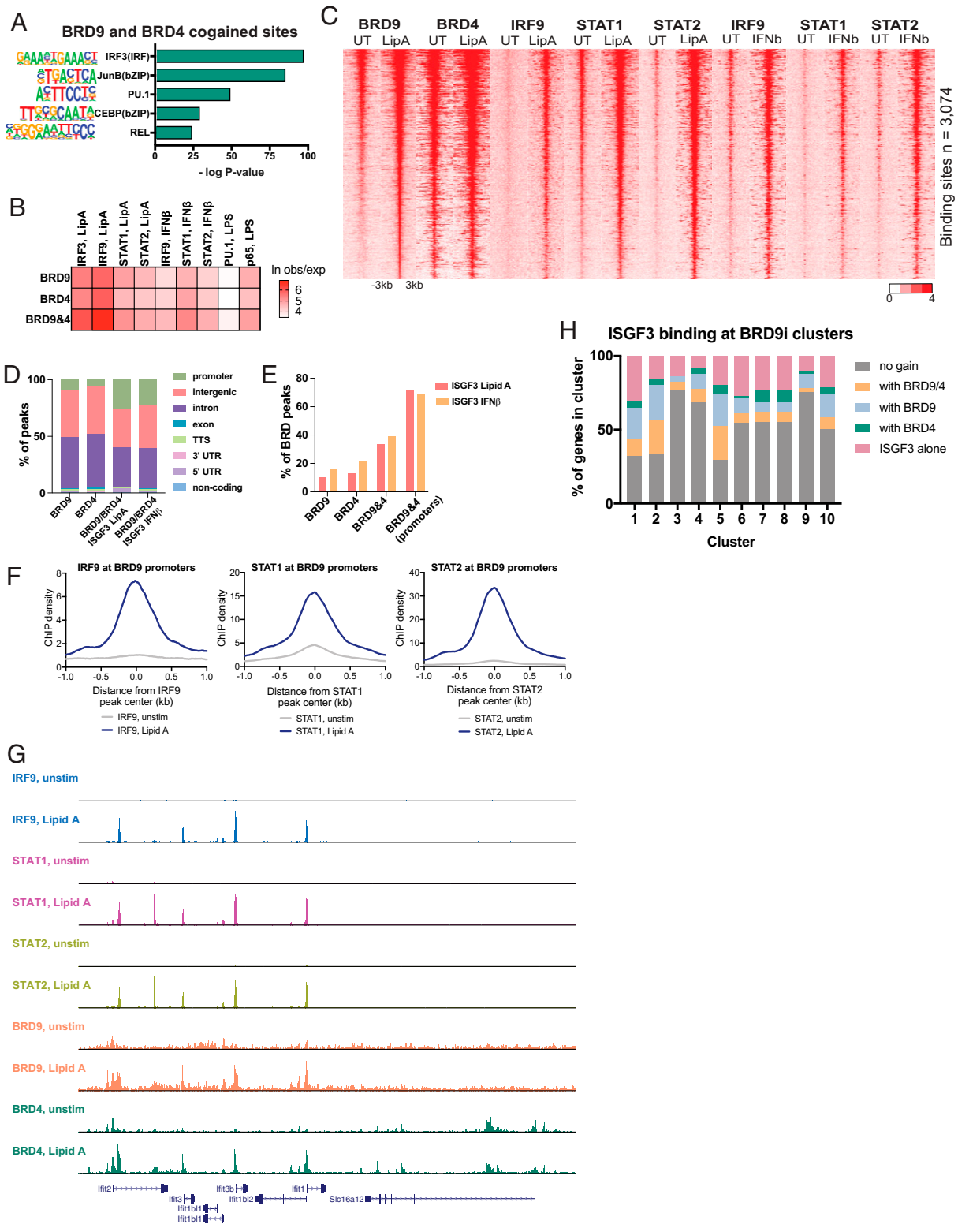

Fig. 4. BRD9/BRD4 are recruited to ISGF3-bound sites in Lipid A- or IFN-α-stimulated BMDMs. (*A*) Significance of enriched motifs for BRD9/BRD4 cogained sites in 4 h Lipid A-stimulated BMDMs. *P* values were calculated using cumulative binomial distribution. (*B*) Cooccurrence analysis showing the natural log of the ratio of the observed/expected number of overlapping peaks for BRD9, BRD4, and BRD9/4 Lipid A-gained sites against in-house-generated ChIP-seq data of ISGF3 and publicly available ChIP-seq data of IRF3, PU.1, p65, and ISGF3 under the indicated stimulations. (*C*) Heat map of BRD9, BRD4, IRF9, STAT1, and STAT2 ChIP signal ± 3 kilobases (kb) centered on the BRD9 peak, ranked according to BRD9 read density at BRD9 Lipid A-gained sites. (*D*) Genomic annotation of gained BRD9 sites, gained BRD4 sites, and cogained BRD4/9 with ISGF3 in Lipid A- or IFN-β-stimulated conditions. (*E*) Percent overlap of BRD peaks with ISGF3 for BRD9, BRD4, BRD9/4 cogained sites, and BRD9/4 cogained sites annotated to promoters. (*F*) Histograms of IRF9, STAT1, and STAT2 ChIP-seq tag density ± 1 kb at BRD9 Lipid A-gained sites annotated to promoters in unstimulated or Lipid A-stimulated conditions (n = 295). (*G*) Genome browser view of ISG *IFIT* locus and non-ISG *Slc16a12*. ChIP-seq results for BRD9, BRD4, IRF9, STAT1, and STAT2 are shown in unstimulated and Lipid A-stimulated conditions. (*H*) ISGF3 binding with BRD9, BRD4, BRD9/4, or alone at RNA-seq gene clusters from Fig. 1*A*.

A and IFN-β stimulation. Indeed, of the BRD9 and BRD4 cogained sites that annotated to promoters, ∼70% of those sites were also bound by the ISGF3 complex, suggesting that when BRD9 and BRD4 are bound at promoters, they are very often found cobound with ISGF3 in Lipid A or IFN-β conditions (Fig. 4*E*). IRF9-, STAT1-, and STAT2-binding increased in response to Lipid A stimulation at BRD9-bound promoters (Fig. 4*F*) as exemplified by a cluster of IFN response genes (*Ifit1*, *Ifit2*, *Ifit3*, *Ifit3b*, *Ifit1bl1*, and *Ifit1bl2*), in which we observed stimulus-dependent binding of ISGF3, BRD9, and BRD4 at the promoter regions of these ISGs (Fig. 4*G*). This is in contrast to nonregulated BRD4 binding at the promoter and intronic regions of the neighboring non-ISG *Slc16a12* locus in the absence of BRD9, STAT1, STAT2, and IRF9, indicating the corecruitment of BRD9 and BRD4 to promoters may be specific to ISGs. Finally, we compared our gene expression data with ChIP-seq data of BRD9, BRD4, and ISGF3. We examined how many sites bound by ISGF3 alone or with BRD9 and/or BRD4 annotated to genes in clusters 1 though 10 of Fig. 1*A* (Fig. 4*H*). We found that clusters with the highest proportion of BRD9i/dBRD9- and JQ1-affected genes (clusters 1, 2, and 5) also had the highest percentage of genes bound by ISGF3 in association with BRD9 or BRD4. This suggests that the corecruitment of BRD9, BRD4, and ISGF3 to promoters in response to stimulation regulates the expression of ISGs in the IFN response pathway.

Previous reports showed that a number of ISGs exhibit basal binding of STAT2:IRF9 and are basally transcribed in an IRF9-dependent manner (19, 27, 28). Given the relationship between BRD9 and ISGF3 in stimulation, we wondered whether BRD9 is required for this priming. Indeed, BRD9 was bound at the majority of IRF9-dependent genes in BMDMs defined by Platanitis and colleagues (19) in unstimulated and Lipid A-stimulated conditions (*SI Appendix*, Fig. S2*A*). Further, treatment with BI-9564 or dBRD9 decreased expression of IRF9-dependent genes in unstimulated BMDMs, and a proportion of these were also reduced in Lipid A-stimulated BMDMs (*SI Appendix*, Fig. S2*B*). For example, we found that STAT2, IRF9, and BRD9 are bound at *Zbp1* and *Irf7* promoters and that the expression of these genes is both IRF9-dependent and BRD9-dependent in unstimulated BMDMs (*SI Appendix*, Fig. S2*C*). Thus, our data demonstrate that BRD9 is required for both the priming and induction of ISGs transcribed by STAT2:IRF9 and ISGF3, respectively.

BRD9 Inhibition/Degradation Results in Reduced ISGF3-Binding at ISGs. Given our previous work (14) and the work of others (12) describing a role for the ncBAF complex in stabilizing transcription factor–binding, we examined the effect of BRD9 inhibition on ISGF3 binding in Lipid A-stimulated BMDMs. Differential peak analysis revealed a robust loss of IRF9-, STAT1-, and STAT2-binding in response to BRD9i, dBRD9, and JQ1 treatments (FC 1.5, Poisson P value < 0.0001) (*SI Appendix*, Fig. S3). While the reduced expression of *Ifnb1* and IFN pathway components could contribute to weaker binding of ISGF3 in I-BRD9- and JQ1-treated cells, the reduction observed in BI-9564/dBRD9-treated cells is likely due to a direct effect of BRD9 on ISGF3 binding at cobound sites. In particular, we found that STAT2- and IRF9-binding were affected in a graded manner with BI-9564 < dBRD9/I-BRD9 < JQ1 (Fig. 5 *A* and *B*). In all treatments, we found that the vast majority of DEGs were correlated with decreased binding of IRF9, STAT1, or STAT2 in BRD9i/dBRD9/JQ1-treated BMDMs (Fig. 5*C*), suggesting that loss of transcription factor–binding contributes to reduced expression in the context of these treatments. We highlight our observations in three BRD9-dependent DEGs, *Cd274, Oas2*, and *Bst2*, in which we observed reduction of IRF9, STAT1, STAT2, BRD9, and BRD4 promoter-binding in dBRD9 treatment compared to vehicle in Lipid A-stimulated BMDMs (Fig. 5*D*).

Discussion

While previous studies have shown a specific role for the SWI/SNF chromatin-remodeling complex in the induction of secondary genes following endotoxin stimulation of BMDMs (7, 8), the role of individual SWI/SNF variants (cBAF, PBAF, and ncBAF) in this response is not known. Here, we show that bromodomain inhibition or degradation of BRD9 prior to Lipid A stimulation results in reduced ISG induction, similar to BET protein inhibition. These data are consistent with previous reports demonstrating a role for BRG1 in ISG induction following type I (29, 30) or type II (31) IFN stimulation but demonstrate a specific role for BRD9 of the ncBAF complex.

Despite correlation between the transcriptional effects of each BRD9 inhibitor and *Brd9* genetic deletion in stimulated macrophages, BI-9564, dBRD9, and I-BRD9 differ vastly in the magnitude of their effect on transcription. I-BRD9 and JQ1 exhibited highly overlapping effects on gene expression, while BI-9564 and dBRD9 resulted in a more-modest reduction in a subset of the genes affected by I-BRD9 and JQ1. These results may reflect the activity of I-BRD9 on other bromodomain-containing proteins (15), including BRD4, or a distinct mechanism of action for I-BRD9. Mapping the binding of BRD9 and BRD4 in the context of BRD9i, dBRD9, and JQ1 shed some light on these possible explanations. For example, we found that BRD4 was similarly displaced from chromatin in I-BRD9- and JQ1-treated cells, likely reflecting off-target effects of I-BRD9 and explaining the similarities between I-BRD9 and JQ1 on gene expression. In contrast, BI-9564 and dBRD9 preferentially affected BRD9-binding. However, for all the inhibitors, we observed loss of both BRD9 and BRD4 at a number of BRD9/BRD4 cobound sites. That is, JQ1 disrupted BRD9 binding in addition to BRD4-binding, while BRD9i/dBRD9 resulted in reduced BRD4 (and BRD9)-binding. These data suggest that individual inhibitors act to displace both the target and its associated partner or potentially that BRD9 and BRD4 exhibit reciprocal dependence on each other for binding at a subset of sites. Notably, loss of BRD9 alone or BRD9/BRD4 occurs at a number of BRD9/BET-dependent DEGs, including genes in the IFN-γ and IFN-α pathways, suggesting that BRD9-binding and coassociation with BRD4 is an important feature of ISG induction.

BRD9 and BRD4 are cobound in unstimulated BMDMs and corecruited to ISG promoters along with ISGF3 following Lipid A stimulation. A recent report identified proximity-labeling of STAT2 with BRD9 in IFN-α-stimulated A549 cells (32). These data suggest that STAT2 or another ISGF3 component may recruit ncBAF complexes to chromatin, which is consistent with BRD9 cobinding with STAT2:IRF9 at the promoters of IRF9-dependent genes in the absence of stimulation, in which we found that BRD9 was required for the basal expression and priming of these genes. We further find that BRD9i/dBRD9 result in reduced ISGF3-binding following Lipid A stimulation. Given that BI-9564 and dBRD9 do not affect IFN-β secretion or the expression of ISGF3 components, these data indicate that BRD9 stabilizes ISGF3 transcription factor–binding directly at cobound sites, similar to what we and others have observed in other cell systems (12, 14). As both ISGF3 and BRD4 (33–37) have been implicated in transcriptional elongation, we favor the model that BRD9 and ncBAF complex localization to promoters affects ISGF3-binding and, in some cases, BRD4-binding, resulting in reduced transcriptional output.

The clinical application of epigenetic inhibitors in cancer and immunity is of great interest. Here, we find a potential role for BRD9 inhibitors and degraders in reducing ISG expression

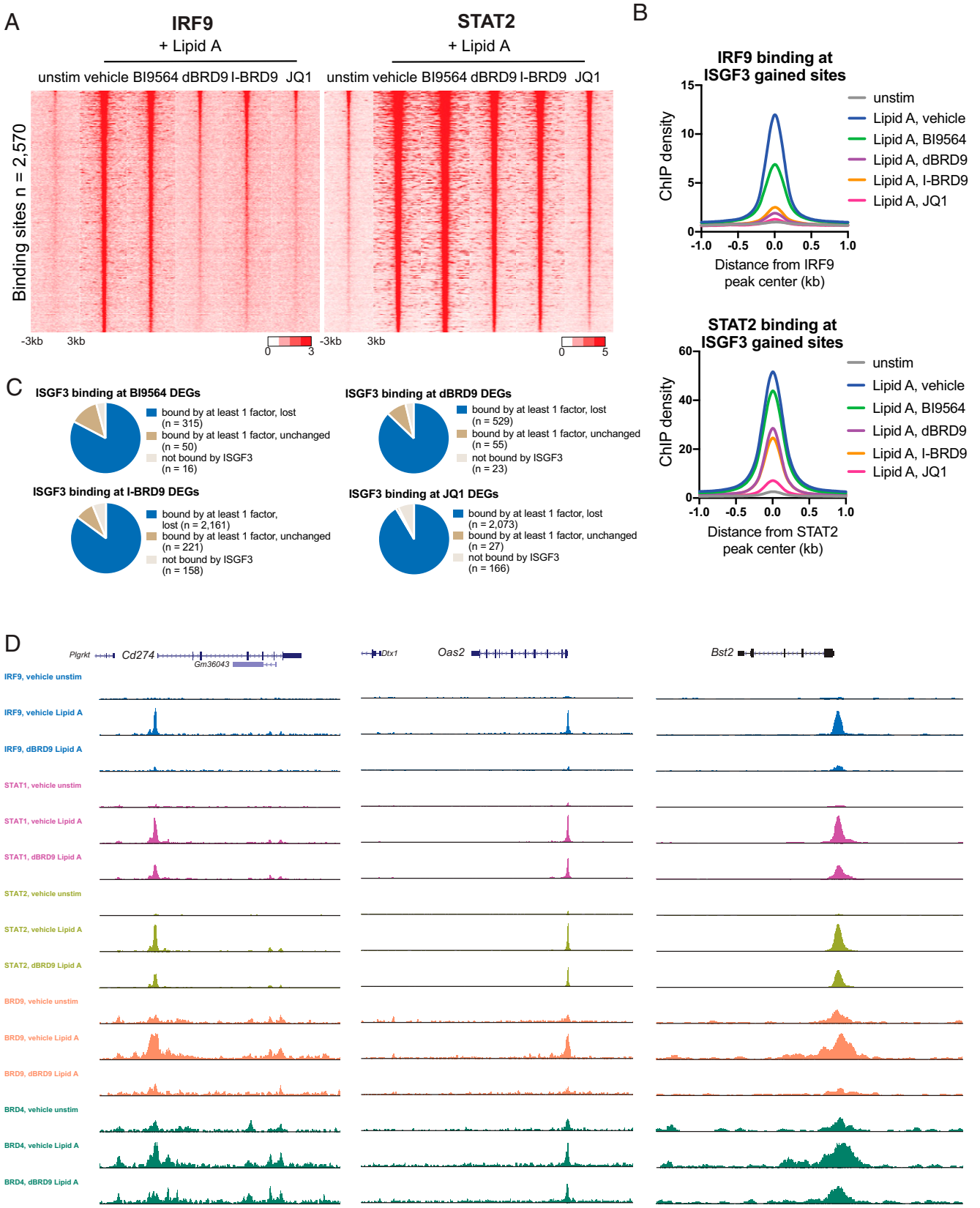

Fig. 5. BRD9i/dBRD9 reduce ISGF3 binding in Lipid A-stimulated BMDMs. (*A*) Heat map of IRF9 and STAT2 ChIP signal ± 3 kilobases (kb) in the presence of BI-9564, dBRD9, I-BRD9, and JQ1 in unstimulated and Lipid A-stimulated BMDMs, ranked according to STAT2 read density at ISGF3 Lipid A-gained sites. (*B*) Histograms of IRF9 and STAT2 ChIP-seq tag density ± 1 kb at ISGF3-binding sites in Lipid A in BRDi conditions. (*C*) Pie chart showing the number of BI-9564, dBRD9, I-BRD9, and JQ1 Lipid A DEGs that are bound by least factor of the ISGF3 complex and those that lose binding upon corresponding inhibitor treatment. (*D*) Genome browser view of *Cd274*, *Oas2*, and *Bst2* locus showing ChIP reads for IRF9, STAT1, STAT2, BRD4, and BRD9 in unstimulated and Lipid A-stimulated conditions with dBRD9.

during inflammation, with dBRD9 and BI-9564 having a more selective effect than I-BRD9. While type I IFN is critical for effective antiviral immunity, it is also implicated in autoimmunity and chronic inflammation (20), settings in which BRD9 modulators could be efficacious in reducing inflammation.

Materials and Methods

BMDM Isolation. Bone marrow was harvested from the femurs and tibias of 8- to 15-wk-old mice and cultured in RPMI-1640 supplemented with 30% Macrophage Colony-Stimulating Factor (M-CSF) and 20% fetal bovine serum (FBS) on Petri dishes. After 6 d, cells were lifted using cold phosphate-buffered saline (PBS) and replated onto tissue culture–treated dishes in half M-CSF media and half Dulbecco's modified Eagle's medium supplemented with 10% FBS.

IFN-β Reporter Assay. RAW-Dual (IRF-Lucia/KI-[MIP-2]SEAP) reporter cells were acquired from Invivogen (https://www.invivogen.com/raw-dual). Cells were cultured according to manufacturer's instructions. For IFN-β activity assay, cells were plated at a density of 2×10^5 cells in a 96-well plate. After 8 h, media was removed and supernatants from BMDMs pretreated with inhibitors and stimulated for 10 h with Lipid A were added to cells and were incubated for 18 to 24 h. Luminescence was read using the Tecan Infinite M1000 Pro plate reader.

RNA-Seq. In total, 1×10^6 BMDMs were pretreated with 500 nM JQ1 (Tocris 4499), 3 μM dBRD9 (Tocris 6606), 3 μM BI9564 (Tocris 5590), or 10 μM I-BRD9 (Tocris 5591) 24 h prior to treatment with DMSO or 100 ng/mL of Lipid A for 0, 1, or 4 h. RNA was extracted and purified with the Zymo Research Quick-RNA miniprep kit according to manufacturer's instructions. RNA-seq libraries were prepared using Illumina TruSeq Stranded messenger ribonucleic acid (mRNA) kit following manufacturer's instructions with 5 μg of input RNA.

RNA-Seq Analysis. Paired-end 42-bp, paired-end 75-bp, or single-end 75-bp reads were aligned to mm10 using Spliced Transcripts Alignment to a Reference (STAR) alignment tool (version 2.5). RNA expression was quantified as raw integer counts using analyzeRepeats.pl in Hypergeometric Optimization of Motif EnRichment (HOMER) using the following parameters: -strand both -count exons -condenseGenes -noadj. DEGs were identified with getDiffExpression.pl in HOMER (cut-offs were set at log2 FC = 0.585 and false discovery rate (FDR) at 0.05 [Benjamin–Hochberg]). GSEA was performed on DEGs against HALLMARK gene sets (GSEA homepage [http://www.gsea-msigdb.org/], 2004 to 2017). For GSEA enrichment plots, GSEA software was used to perform the analyses with the following parameters: number of permutations = 1,000; enrichment statistic = weighted; and metric for ranking of genes = difference of classes (input RNA-seq data were log transformed). For Fig. 1 *C* and *D*, correlation of RNA-seq log2 fold-change values between datasets was assessed by plotting the goodness of fit (R^2) values in GraphPad Prism Version 7. For RNA-seq kinetic heat map, genes were clustered by k-means clustering (default settings, 10 clusters, 100 runs, and centered correlation) using Cluster 3.0 software (https://bonsai.hgc.jp/~mdehoon/software/cluster/).

ChIP-Seq Sample Preparation. In total, 10 to 15 million BMDMs were pretreated overnight with 500 nM JQ1; 3 μM dBRD9; 3 μM BI9564; or 10 μM I-BRD9 prior to treatment with DMSO or 100ng/mL of Lipid A for 4 h. For ChIP-seq in RAW264.7, cells were treated with either DMSO or Lipid A for 4 h. Cells were cross linked in 3 mM disuccinimidyl glutarate for 30 min then in 1% formaldehyde for 10 min at room temperature. After quenching with 125 mM glycine, the cells were washed in 1× PBS, pelleted, flash frozen in liquid nitrogen, and stored at −80 °C. Cell pellets were thawed on ice and incubated in lysis solution (50 mM Hepes KOH pH 8, 140 mM NaCl, 1 mM ethylenediamine tetraacetic acid (EDTA), 10% glycerol, 0.5% Nonidet P-40, and 0.25% Triton X-100) for 10 min. The isolated nuclei were washed (10 mM Tris·HCl pH 8, 1 mM EDTA, 0.5 mM EGTA, and 200 mM NaCl) and sheared in (0.1% sodium dodecyl sulfate (SDS), 1 mM EDTA, and 10 mM Tris·HCl pH 8) with the Covaris E229 sonicator for 10 min. After centrifugation, chromatin was immunoprecipitated overnight at 4 °C with 1:100 BRD9 (Active Motif, pAb #61537), 5 μg BRD4 (Bethyl, Rabbit pAb #A301-985A50), BRD2 (Cell Signaling Rabbit mAb #5848S), 1:100 IRF9 (clone 6F1-H4, Millipore mouse mAb #MABS1920), 1:100 STAT1 (Cell Signaling Rabbit pAb #9172S), and 1:100 STAT2 (Cell Signaling Rabbit pAb #72604S). The next day, the antibody-bound DNA was incubated with Protein A+G Dynabeads (Invitrogen) in ChIP buffer (50 mM Hepes KOH pH 7.5, 300 mM NaCl, 1 mM EDTA, 1% Triton X-100, 0.1% sodium deoxycholate, and 0.1% sodium dodecyl sulfate), washed, and treated with Proteinase K and RNase A and reverse cross linked. Purified ChIP DNA was used for library generation (NuGen Ovation Ultralow Library System version 2 or NEBNext Ultra II DNA Library Prep Kit for Illumina) according to manufacturer's instructions.

ChIP-Seq Analysis. Single-end 50-bp or 75-bp or paired-end 75-bp reads were aligned to the mouse genome mm10 using STAR alignment tool (version 2.5) (38). ChIP-seq peaks were called using findPeaks within HOMER using -style factor (default settings, except for IRF9 in which peaks were defined as 1.5-fold over input and fourfold over local tag counts with FDR 0.001 [Benjamin–Hochberg]). Differential ChIP peaks were called using getDiffExpression.pl with fold change ≥ 1.5 or ≤ −1.5, Poisson P value < 0.0001. ChIP-seq peaks were annotated by mapping to the nearest transcription start site (TSS) using the annotatePeaks.pl program. Metaplots were generated using annotatePeaks.pl with parameters -size 2000 and -hist 10. Heat map showing overlap of binding sites were generated using mergePeaks in HOMER with flag -matrix, which outputs hypergeometric P values of overlap and the observed/expected ratio of overlap. Heat maps of ChIP-seq signal were performed using the annotatePeaks.pl in HOMER with the following parameters -size 6000 -hist 25 and visualized in Java TreeView (https://jtreeview.sourceforge.net/). For motif-enrichment analysis, findMotifsGenome.pl command was used with -size 200. Random guanine-cytosine (GC) content-matched genomic regions were used as background. Enriched motifs are statistically significant motifs in input over background by a P value of less than 0.05 using cumulative binomial distribution.

Protein Lysis and Western Blot Analysis. BMDMs were pretreated overnight with 500 nM JQ1, 3 μM dBRD9, 3 μM BI9564, or 10 μM I-BRD9 and then stimulated with either DMSO or Lipid A for 4 h. Cells were lysed in radioimmunoprecipitation assay buffer (RIPA) buffer (50 mM Tris pH 8, 150 mM NaCl, 1% Nonidet P-40, 0.5% sodium deoxycholate, and 0.1% sodium dodecyl sulfate) and supplemented with protease and phosphatase inhibitors. Cleared protein lysates were quantified using Bio-Rad Detergent Compatible (DC) Protein Assay (Catalog no. 5000112), supplemented with 4× NuPAGE (polyacrylamide gel electrophoresis) LDS (lithium dodecyl sulfate) Sample Buffer and 0.5M Dithiothreitol (DTT) and boiled for 5 min at 95 °C. A total of 50 μg of total protein was run on an SDS-PAGE 4 to 12% gradient gel, transferred, and incubated overnight with primary antibody in 2% bovine serum albumin (BSA) in PBS solution. Blots were washed four times in 1× PBS with 0.1% Tween20 (PBS-T), incubated with secondary antibody for 1 h at room temperature, washed again, and imaged on the LI-COR Odyssey CLx imager. Western blots were quantified using Image Studio Lite software.

Data Availability. All data has been uploaded to the Gene Expression Omnibus (GEO) database under accession no. GSE176146 (https://www.ncbi.nlm.nih.gov/geo/query/acc.cgi?acc=GSE176146). Publicly available data were processed using HOMER version 4.10 (Christopher Benner, HOMER, http://homer.ucsd.edu/homer/index.html). The following database deposition numbers are given: for RNA-seq of *Irf3*$^{-/-}$, *Ifnar* $^{-/-}$, *Trif* $^{-/-}$, *Myd88* $^{-/-}$, Pam3, and CHX treatment, GEO GSE67355 (2); for RNA-seq of LysM-Cre BRD9 knockout, Sequence Read Archive (SRA) PRJNA731887 (22); for ChIP-seq of IRF3, GEO GSE67357 (2); IRF9, STAT1, and STAT2 in IFNb stimulation, GEO GSE115435 (19); PU.1, GEO GSE38379 (25); and p65, GEO GSE106701 (26).

ACKNOWLEDGMENTS. N.S.A. is supported by the Salk Institute T32 Cancer Training Grant T32CA009370. J.G. was supported by T32CA009370 and GM128377-01. D.C.H. is supported by the NIH (GM128943-01, CA184043-03, and AI151123), the Pew-Stewart Scholars for Cancer Research, and the American Cancer Society Research Scholar Award. This work was also supported by National Cancer Institute–funded Salk Institute Cancer core facilities (CA014195).

1. C. K. Glass, G. Natoli, Molecular control of activation and priming in macrophages. *Nat. Immunol.* **17**, 26–33 (2016).
2. A. J. Tong *et al.*, A stringent systems approach uncovers gene-specific mechanisms regulating inflammation. *Cell* **165**, 165–179 (2016).
3. D. M. Bhatt *et al.*, Transcript dynamics of proinflammatory genes revealed by sequence analysis of subcellular RNA fractions. *Cell* **150**, 279–290 (2012).
4. V. Toshchakov *et al.*, TLR4, but not TLR2, mediates IFN-beta-induced STAT1alpha/beta-dependent gene expression in macrophages. *Nat. Immunol.* **3**, 392–398 (2002).
5. D. C. Hargreaves, T. Horng, R. Medzhitov, Control of inducible gene expression by signal-dependent transcriptional elongation. *Cell* **138**, 129–145 (2009).
6. L. Escoubet-Lozach *et al.*, Mechanisms establishing TLR4-responsive activation states of inflammatory response genes. *PLoS Genet.* **7**, e1002401 (2011).
7. V. R. Ramirez-Carrozzi *et al.*, Selective and antagonistic functions of SWI/SNF and Mi-2beta nucleosome remodeling complexes during an inflammatory response. *Genes Dev.* **20**, 282–296 (2006).
8. V. R. Ramirez-Carrozzi *et al.*, A unifying model for the selective regulation of inducible transcription by CpG islands and nucleosome remodeling. *Cell* **138**, 114–128 (2009).

9. A. Alpsoy, E. C. Dykhuizen, Glioma tumor suppressor candidate region gene 1 (GLTSCR1) and its paralog GLTSCR1-like form SWI/SNF chromatin remodeling subcomplexes. *J. Biol. Chem.* **293**, 3892–3903 (2018).
10. J. Gatchalian *et al.*, A non-canonical BRD9-containing BAF chromatin remodeling complex regulates naïve pluripotency in mouse embryonic stem cells. *Nat. Commun.* **9**, 5139 (2018).
11. B. C. Michel *et al.*, A non-canonical SWI/SNF complex is a synthetic lethal target in cancers driven by BAF complex perturbation. *Nat. Cell Biol.* **20**, 1410–1420 (2018).
12. A. Alpsoy *et al.*, BRD9 is a critical regulator of androgen receptor signaling and prostate cancer progression. *Cancer Res.* **81**, 820–833 (2021).
13. Z. Wei *et al.*, Vitamin D switches BAF complexes to protect β cells. *Cell* **173**, 1135–1149.e15 (2018).
14. C. S. Loo *et al.*, A genome-wide CRISPR screen reveals a role for the non-canonical nucleosome-remodeling BAF complex in Foxp3 expression and regulatory T cell function. *Immunity* **53**, 143–157.e8 (2020).
15. N. H. Theodoulou *et al.*, Discovery of I-BRD9, a selective cell active chemical probe for bromodomain containing protein 9 inhibition. *J. Med. Chem.* **59**, 1425–1439 (2016).
16. L. J. Martin *et al.*, Structure-based design of an in vivo active selective BRD9 inhibitor. *J. Med. Chem.* **59**, 4462–4475 (2016).
17. D. Remillard *et al.*, Degradation of the BAF complex factor BRD9 by heterobifunctional ligands. *Angew. Chem. Int. Ed. Engl.* **56**, 5738–5743 (2017).
18. P. Filippakopoulos *et al.*, Selective inhibition of BET bromodomains. *Nature* **468**, 1067–1073 (2010).
19. E. Platanitis *et al.*, A molecular switch from STAT2-IRF9 to ISGF3 underlies interferon-induced gene transcription. *Nat. Commun.* **10**, 2921 (2019).
20. L. B. Ivashkiv, L. T. Donlin, Regulation of type I interferon responses. *Nat. Rev. Immunol.* **14**, 36–49 (2014).
21. S. Rahman *et al.*, The Brd4 extraterminal domain confers transcription activation independent of pTEFb by recruiting multiple proteins, including NSD3. *Mol. Cell. Biol.* **31**, 2641–2652 (2011).
22. L. Wang *et al.*, Bromodomain containing 9 (BRD9) regulates macrophage inflammatory responses by potentiating glucocorticoid receptor activity. *Proc. Natl. Acad. Sci. U.S.A.* **118**, e2109517118 (2021).
23. A. Dey *et al.*, BRD4 directs hematopoietic stem cell development and modulates macrophage inflammatory responses. *EMBO J.* **38**, e100293 (2019).
24. A. C. Belkina, B. S. Nikolajczyk, G. V. Denis, BET protein function is required for inflammation: Brd2 genetic disruption and BET inhibitor JQ1 impair mouse macrophage inflammatory responses. *J. Immunol.* **190**, 3670–3678 (2013).
25. R. Ostuni *et al.*, Latent enhancers activated by stimulation in differentiated cells. *Cell* **152**, 157–171 (2013).
26. A. Horvath *et al.*, Labelled regulatory elements are pervasive features of the macrophage genome and are dynamically utilized by classical and alternative polarization signals. *Nucleic Acids Res.* **47**, 2778–2792 (2019).
27. W. Wang *et al.*, Unphosphorylated ISGF3 drives constitutive expression of interferon-stimulated genes to protect against viral infections. *Sci. Signal.* **10**, eaah4248 (2017).
28. B. Testoni *et al.*, Chromatin dynamics of gene activation and repression in response to interferon alpha (IFN(alpha)) reveal new roles for phosphorylated and unphosphorylated forms of the transcription factor STAT2. *J. Biol. Chem.* **286**, 20217–20227 (2011).
29. H. Liu, H. Kang, R. Liu, X. Chen, K. Zhao, Maximal induction of a subset of interferon target genes requires the chromatin-remodeling activity of the BAF complex. *Mol. Cell. Biol.* **22**, 6471–6479 (2002).
30. M. Huang *et al.*, Chromatin-remodelling factor BRG1 selectively activates a subset of interferon-alpha-inducible genes. *Nat. Cell Biol.* **4**, 774–781 (2002).
31. Z. Ni *et al.*, Apical role for BRG1 in cytokine-induced promoter assembly. *Proc. Natl. Acad. Sci. U.S.A.* **102**, 14611–14616 (2005).
32. J. Börold *et al.*, BRD9 is a druggable component of interferon-stimulated gene expression and antiviral activity. *EMBO Rep.* **22**, e52823 (2021).
33. M. K. Jang *et al.*, The bromodomain protein Brd4 is a positive regulatory component of P-TEFb and stimulates RNA polymerase II-dependent transcription. *Mol. Cell* **19**, 523–534 (2005).
34. Z. Yang *et al.*, Recruitment of P-TEFb for stimulation of transcriptional elongation by the bromodomain protein Brd4. *Mol. Cell* **19**, 535–545 (2005).
35. G. E. Winter *et al.*, BET Bromodomain Proteins Function as Master Transcription Elongation Factors Independent of CDK9 Recruitment. *Mol. Cell* **67**, 5–18.e19 (2017).
36. M. C. Patel *et al.*, BRD4 coordinates recruitment of pause release factor P-TEFb and the pausing complex NELF/DSIF to regulate transcription elongation of interferon-stimulated genes. *Mol. Cell. Biol.* **33**, 2497–2507 (2013).
37. I. Marazzi *et al.*, Suppression of the antiviral response by an influenza histone mimic. *Nature* **483**, 428–433 (2012).
38. A. Dobin *et al.*, STAR: Ultrafast universal RNA-seq aligner. *Bioinformatics* **29**, 15–21 (2013).